Surface Reconstruction and Feature Detection on 3-D Images of Dental Imprints

Marielle Mokhtari and Denis Laurendeau

†Département de Génie Électrique
Faculté des Sciences et Génie
Université Laval
Québec, (Qué), Canada, G1K 7P4

Abstract / Résumé

This paper presents a computer vision approach for the reconstruction of teeth on the 3-D image of a wax dental imprint. The reconstructed teeth are processed in order to detect feature points on each tooth. The features of interests are cusps on molars, premolars and canines. These features are detected by a scale-space approach called the *watershed* algorithm. These points are used to measure a set of orthodontic parameters for automatic diagnosis of malocclusion problems. The ultimate goal of the approach is to devise an autonomous expert system for epidemiological studies in orthodontics. Such system can play a significant role in the prevention of dental abnormalities at an early age of the patient and help to follow the evolution of the treatment.

Cet article présente une approche de vision par ordinateur pour la reconstruction des dents sur l'image d'une empreinte dentaire en cire. Les dents reconstruites sont ensuite traitées dans le but de repérer des points particuliers sur chaque dent. Les points particuliers sont notamment les pointes des molaires, prémolaires et canines. Ces points sont détectés grâce à une approche multi-échelles appelée algorithme du *watershed*. Le but final du projet est la mise au point d'un système expert pour les études épidémiologiques en orthodontie. Un tel système peut jouer un rôle significatif dans la prévention des malocclusions dentaires tout en permettant un suivi de l'évolution du traitement orthodontique.

Introduction

The detection and correction of development of malocclusions and other dental abnormalities is a very important task of orthodontic diagnosis. At present, the diagnosis is based on the observation of a plaster model of the mouth. However, the measurement of the plaster models is costly, complex and is a painful operation for the patient. Furthermore, the diagnosis does not rely on objective measurements but rather on subjective interpretation of the shape of the model.

This paper presents a subject of a computer vision system for processing of the 3-D profile of a wax dental imprint. The wax imprint is easier to record and cheaper than a plaster model. The system aims at measuring a set of ten orthodontic parameters (defined by a team of researchers at the School of Dentistry of Laval University)[6] that are fed to an expert system for objective diagnosis of malocclusion problems.

As shown in Figure 1, the computer vision system comprises a 3-D camera based on the absorption of light by a diffusing medium and software modules for the processing of the 3-D data which comprises *i)* a sensor fusion algorithm for the refinement of raw 3-D images, *ii)* algorithms for the detection of interstices between teeth and the identification of teeth, *iii)* a surface reconstruction algorithm for the analytic description of the shape of each type of tooth and *iv)* a module for the extraction of feature points on each tooth. This paper

Figure 1 Different modules of the computer vision system for orthodontic diagnosis.

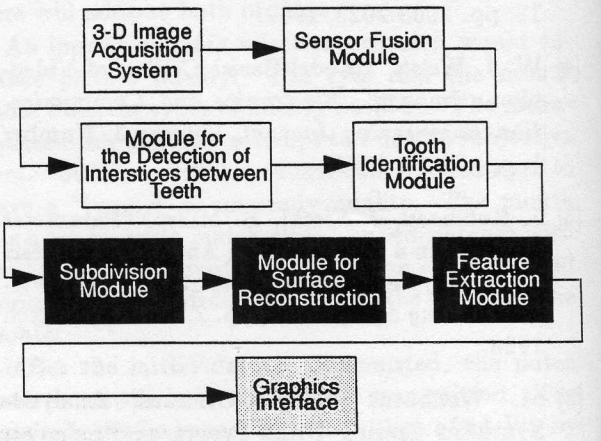

presents the modules enclosed in black boxes in Figure 1 and is organized as follows. First the four top modules in Figure 1 are presented briefly in Section 1. Then, the subdivision of the dental imprint image into connected regions is discussed in Section 2. The surface of each recovered tooth is reconstructed with uniform cubic smoothing splines as described in Section 3. The extraction of feature points on the reconstructed profile of the teeth is detailed in Section 4. Finally, Section 5 presents the result of experiments on several dental imprints, discusses the improvements that could be brought to the system, and describes the next steps in the development of the system.

1 . Background material

This section presents briefly the acquisition strategy for the measurement of the 3-D profile of a wax dental imprint as well as the sensor fusion module which allows to significantly reduce the noise level in the raw 3-D image. The software module for the detection of the interstices between the teeth and for the identification of the teeth on the imprint are also covered.

1.1 Image Acquisition

The 3-D images of the wax dental imprint are obtained from a technique based on the differential absorption of light by a diffusing medium. Figure 2 shows the

Figure 2 Diagram of the acquisition setup for the measurement of the 3-D profile of a dental imprints.

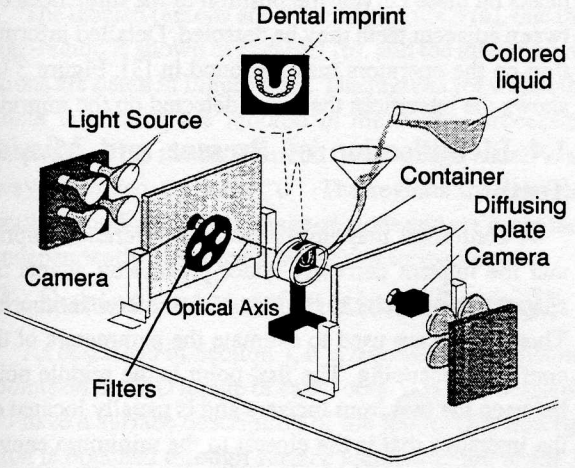

different components of the acquisition system. The dental imprint is immersed in a container filled with colored liquid. The absorption spectrum of the liquid shows an absorption peak at 625 nm and is transparent to other wavelengths. A standard CCD camera is placed on each side of the container and observes one side of the imprint which is illuminated by a lighting system composed of 6 halogen bulbs. A first image of the imprint is taken at a wavelength λ_1 = 600 nm which is absorbed by the liquid[1]. A second image is then taken at a wavelength λ_2 = 750 nm which is not absorbed by the liquid. This image is simply an illuminance image of the imprint and is in perfect alignment with the image at λ_1 = 600 nm. Range is computed at each pixel using the following line of reasoning. The illuminance of a point at the surface of the imprint and imaged at pixel (i,j) on the camera is, at wavelength λ_1, and near the optical axis of the camera:

$$dE_{\lambda_1}(i,j) = K_1 \cos(\phi(i,j))\, e^{-2az(i,j)} \quad (1)$$

where ϕ is the orientation of the normal to the surface at this point, z is the depth of the point in the liquid and K_1 is a constant. At wavelength λ_2, the illuminance of the same point is:

$$dE_{\lambda_2}(i,j) = K_2 \cos(\phi(i,j)) \quad (2)$$

where K_2 is a constant. Range is obtained by taking the ratio between Eq (1) and Eq (2):

$$z(i,j) = \frac{1}{2\alpha}\left(ln\left[\frac{dE_{\lambda_2}(i,j)}{dE_{\lambda_1}(i,j)}\right] + ln\left[\frac{K_1}{K_2}\right]\right) \quad (3)$$

Parameters K_1, K_2 and α in Eq (3) are obtained from a calibration procedure. Details of the calibration procedure may be found in [3]. Figure 3 shows a dental imprint (a) and the raw 3-D image of a molar (b) obtained with Eqs (1)-(3).

1.2 Noise Reduction Through Sensor Fusion

Since Eq (3) involves a division between two images, the noise level is sometimes important, especially near the bottom of the teeth. However, it is possible to use a shape-from-shading algorithm to improve range values in the 3-D images. It is a well-known fact that shape-from-shading fails to reveal the concavity or convexity of a surface from the shading equations alone [5]. However, as stated in Section 1.1, the 3-D image and the image taken at λ_2 (illuminance image) are in perfect registration. The 3-D image can thus be used as an initial estimate of the 3-D shape. A shape-from-shading algorithm is applied to the illuminance image and progressively refines the 3-D image through a relaxation technique. The flow chart of the fusion module is shown in Figure 4. More details on the fusion module may be

1. An optical filter is automatically placed in front of the camera under computer control.

Figure 3 Results of the first processing steps of the dental imprint processing system.

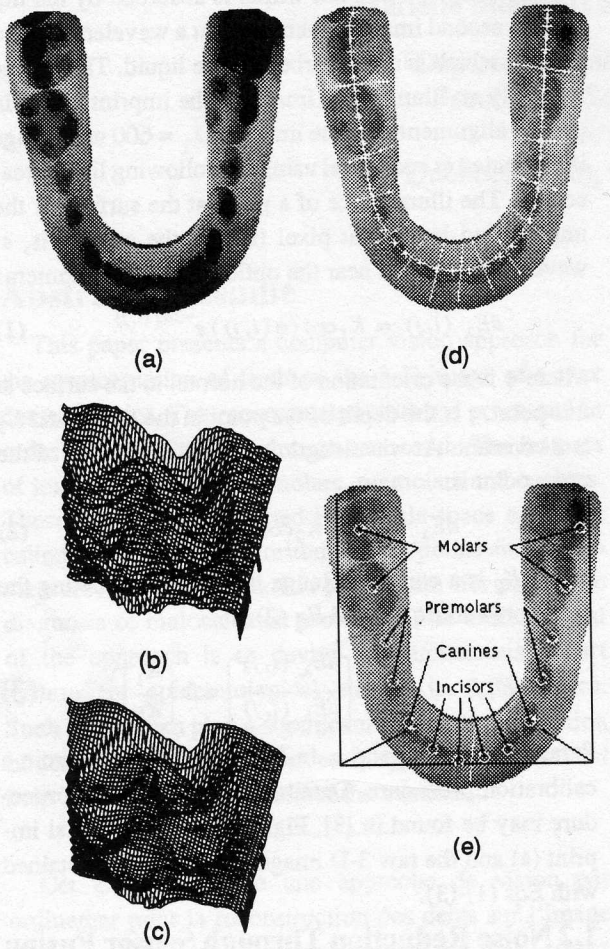

found in [8]. Figure 3 (c) shows the result of the fusion algorithm on the molar of Figure 3 (b)[1].

1.3 Detection of the Interstices Between Existing Teeth

The range images obtained from the fusion algorithm are processed in order to extract the position of each tooth on both arches. It was found that it is very difficult to attempt to find each tooth directly since the bite may vary from imprint to imprint, teeth might be missing, etc. We rather search for the interstices between the teeth and then identify the type of tooth from the location of the interstices.

First, the central axis of the imprint is detected (see the "+" signs in Figure 3 (d)). This axis is swept from left

1. The same algorithm is applied to the complete imprint. Only the molar is shown due to space limitation.

Figure 4 Flow chart of the noise reduction module using sensor fusion between the 3-D image and the illuminance image.

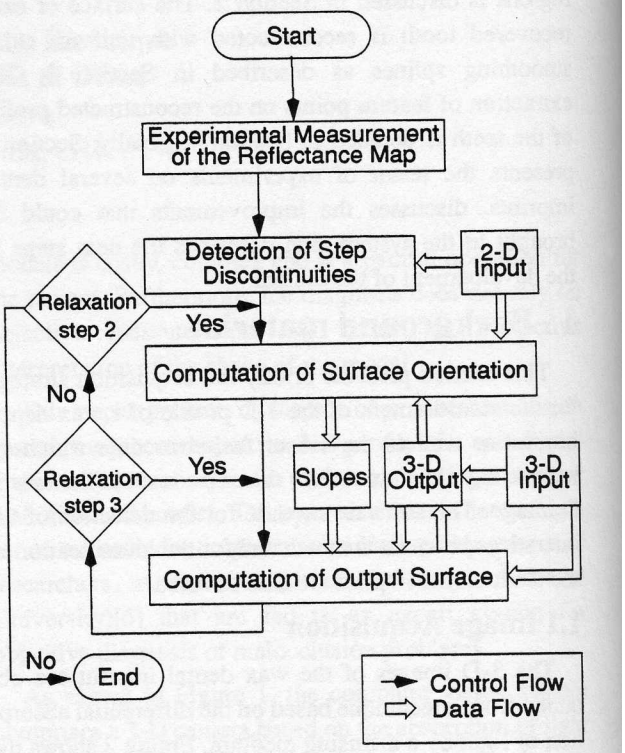

to right with a set of operators that yield characteristic curves of the imprint along the axis. By detecting the peaks on these curves, the position of the interstices between adjacent teeth may be detected. Detailed information on the operators may be found in [3]. Figure 3 (d) shows the interstices that were detected on the imprint.

1.4 Identification of Present and Missing Teeth

A conformal mapping between a reference imprint and the imprint currently under processing adapts the shape of the imprint to the one of the reference imprint. Three points are used to estimate the parameters of the conformal mapping. The first point is the middle point between the two front incisors and is usually located on the interstice that is the closest to the minimum central point on the curved axis (see Figure 3 (e)). This choice is motivated by the fact that the majority of arches have their incisors, which is not always the case for molars and premolars. The two other points are located at the peak of the two canines which are the most strategic teeth in the mouth [7]. Figure 3 (e) shows the teeth that were identified on the imprint. Detailed information on

the operators may be found in [1].

2 . Labeling of the dental imprint in connected regions

The information that is available following the previous processing steps is:

1-the position of the interstices between teeth and,

2-the *approximate* location of the teeth on the imprint.

In order to reduce the area that has to be processed for the extraction of feature points on each tooth, the imprint is labeled into regions occupied by a single tooth, based on the information mentioned in 1 and 2 above. The regions are bounded by one or two interstice(s) and the lingual and buccal sides of the imprint. Each region is assigned a different label and it is determined whether the region comprises a tooth or not using the information provided by conformal mapping. A list of regions is built and the following attributes are included in each list entry:

1-the coordinates of the upper left and lower right corners of the circumscribing rectangle of the region,

2- presence or absence of a tooth in the circumscribing rectangle,

3- type of tooth of the region (in case a tooth is present).

The labeled regions are shown in Figure 5 (a), one image-region is shown in Figure 5 (b), and the identified regions are listed in Figure 5 (c). The regions for which the tooth is missing are ignored in the further processing steps as well as the background of the image which is always assigned the label "0". The regions that circumscribe a tooth are called image-regions and are processed independently using the approach described below.

3 . Surface reconstruction of a tooth

As described in Section 4, it is required to find feature points on the 3-D image of each tooth. It is thus desirable to have a surface description of the tooth. This description is obtained through surface reconstruction of the 3-D profile of the tooth with uniform cubic B-splines. This reconstruction has the advantage that it interpolates the 3-D coordinates of the raw range image and thus provides a better estimate of the position of the feature points. It also performs low-pass filtering of the data.

The parametric equation of the two-dimensional uniform cubic B-spline is given by:

Figure 5 (a) Labeling of the regions, (b) one image-region and (c) identification of the regions on the imprint.

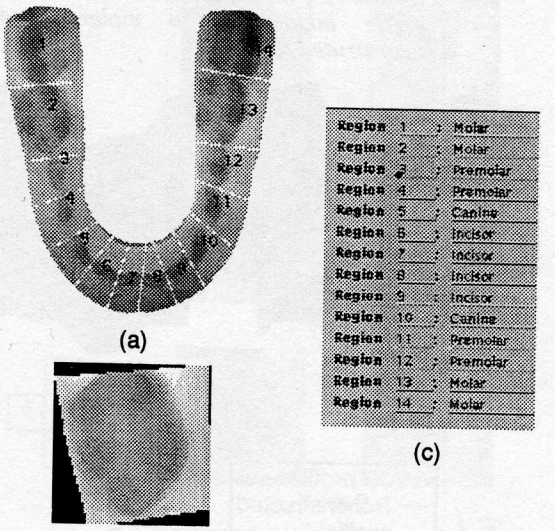

$$S(u,v) = \sum_i \sum_j P_{i,j} \, B_{i,j}(u,v) \qquad (4)$$

where $u = x$, $v = y$, P_{ij} is the control point matrix composed of the original data (raw $z(x,y)$ coordinates) and $B_{ij}(u,v) = B_{ij}(u) \times B_{ij}(v)$ is the tensor product of two one-dimensional uniform B-spline functions defined along each coordinate axis [2].

Each labeled region is processed in turn and the surface of the area corresponding to the imprint is reconstructed using Eq (4). Figure 6 (a) shows the 3-D surface of a molar and Figure 6 (b) shows the reconstructed surface using uniform cubic B-spline. The smoothing of the raw image profile in Figure 6 (c) is visible on the reconstructed profile of Figure 6 (d). The smoothed surface is resampled at each (x,y) coordinate of the parametric plane and this data is used for the detection of the feature points on each tooth.

4 . Detection of feature points on the reconstructed teeth

The feature points that are used for the measurement of the orthodontic parameters are mostly the cusps (e.g. peaks) of the molars and premolars and the apex of the canines.

4.1 Basic Notions of Dental Anatomy

It is important to briefly describe the anatomy of the various teeth prior the description of the algorithm for

Figure 6 Surface reconstruction with uniform cubic B-splines. (a) shows the raw 3-D image of a molar and (b) shows the reconstructed image. (c) shows the comparison between a 3-D profile including two molars and its reconstruted shape.

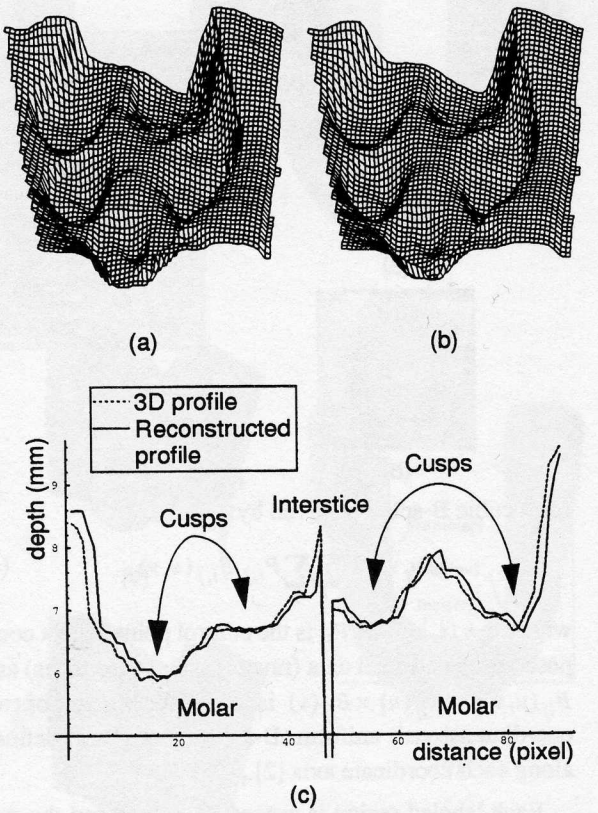

the detection of feature points. In the following, the number of teeth of each type refers to a single arch.

First, the two canines have a simple conical shape. An important feature point of the canine is the apex which is the tip of the cone (see Figure 7). In the set of orthodontic parameters that have to be measured on the imprint, the apex is the only feature point that is needed [6].

The four premolars are generally *bicuspids* which means that they show two cusps separated by a ridge (see Figure 7). However, only the cusp with the largest depth is used for the measurement of the orthodontic parameters.

The four molars may have between three to four major cusps for the maxillary arch and between three to five cusps for the mandibular arch[1] (see Figure 7) that are all used for the measurement of the orthodontic parameters.

1. The maxillary arch is part of the cranium and is an immovable apart from it. The mandibular arch is part of the lower jaw and is a movable part of the skull [7].

It is important to mention that even though the two wisdom teeth are molars, they are not used for the measurement of orthodontic parameters since they are the most variable anatomically and developmentally.

Figure 7 Feature points on canine, premolars and molars shown by arrows in grey-scale for a mandibular arch (Diagram reprinted from [7]).

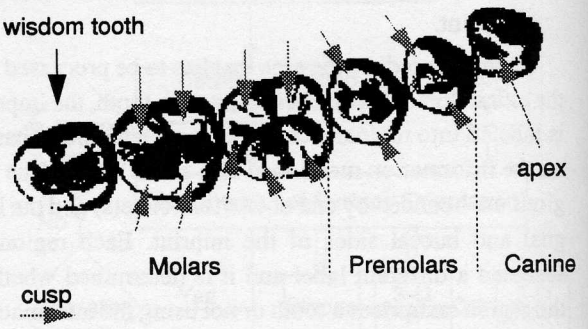

4.2 Detection and Validation of Local Minima on the Reconstructed 3-D profile of Molars, Premolars and Canines

Since the measurement of orthodontic parameters requires the detection of the apex of each canine, the detection of at least one cusp on each premolar, and the detection of each cusp on each molar, an algorithm for the detection of local minima has been designed. The algorithm is a multi-scale *watershed* approach which detects the position of the cusps at several scales and then validates the position of each cusp using a scale-space analysis.

4.2.1. Pre-processing of the reconstructed 3-D image of each tooth

Even though the image has been filtered with the spline fit described in Section 3, there still remain local peaks caused by noise which corrupt the profile and can cause the detection of false minima. To reduce the effect of local disturbances caused by these spikes, a 3 x 3 median filter is applied to the reconstructed profile. The filtered image is then fed to the *watershed* algorithm described in 4.2.2.

4.2.2. The multi-scale *watershed* algorithm for minima detection

The detection of minima is not a trivial problem in mathematical function analysis. In most applications, one is concerned with the detection of the *global* minimum among a set of *local* minima. In this particular application, the problem is even more complex since *all*

valid minima (e.g. cusps or apexes) must be detected and validated. The use of absolute thresholds is ruled out since the shape and size of the imprints vary too much to allow efficient threshold selection. The detection of the zero-crossings of the second derivative of the reconstructed surface has also shown to be too noisy to allow robust minima detection. To avoid these problems, a multi-scale *watershed* strategy has thus been implemented for the detection of local minima. The strategy is comprised of three major steps:

1-the reconstructed surface of a tooth is smoothed at four different levels by a 4-neighbour averaging template. This creates *four layers*, each layer being obtained from the previous one. Figure 8 (a) shows the averaging operator that is used to construct the 4-layer structure. Figures 8 (b) and (c) show two images of a molar of the mandibular arch at each layer,

2- since the variation in range of the 3-D data is small (4 mm max) on an imprint, the range values of *each layer* are remapped on a 256-level scale in order to increase the dynamic range,

3- the watershed algorithm is then applied to *each layer* in order to detect potential minima.

The watershed algorithm comprises two steps: *i)* an initialization step and *ii)* an iterative step.

For the initialization step, a threshold $\tau = 0$ is applied to the remapped range image and a binary image is generated. The pixel with $z = \tau$ is assigned the value *1*, and other pixels are assigned the value *0*. For $\tau = 0$, this pixel is the bottom pixel of the image and is assumed to be the position of the global minimum of the lower cusp. The coordinates of this minimum are stored as the top element of a list of minima *min_list*.

Following the initialization step, the iterative step begins. The threshold is increased such as $\tau = \tau + 1$. The pixels with $z \leq \tau$ are assigned the value *1*, and other pixels are assigned the value *0*. The connected regions in the binary image are detected and labeled. The number of detected regions is stored in a counter num_reg (τ). If num_reg $(\tau - 1) \geq$ num_reg(τ), this means that no new regions have appeared or that regions at the preceding stage have merged. Then τ is increased and a new thresholding iteration begins.

If num_reg $(\tau - 1) <$ num_reg (τ), this means that new regions have appeared in the binary image and that new local minima must be processed. The coordinates of elements on *min_list* are inspected and those falling within the frontiers of a detected region are not recomputed. The coordinates of the center of gravity of the new regions are added to *min_list*.

Figure 8 Detection and localization of local minima (cusps) on two molars.

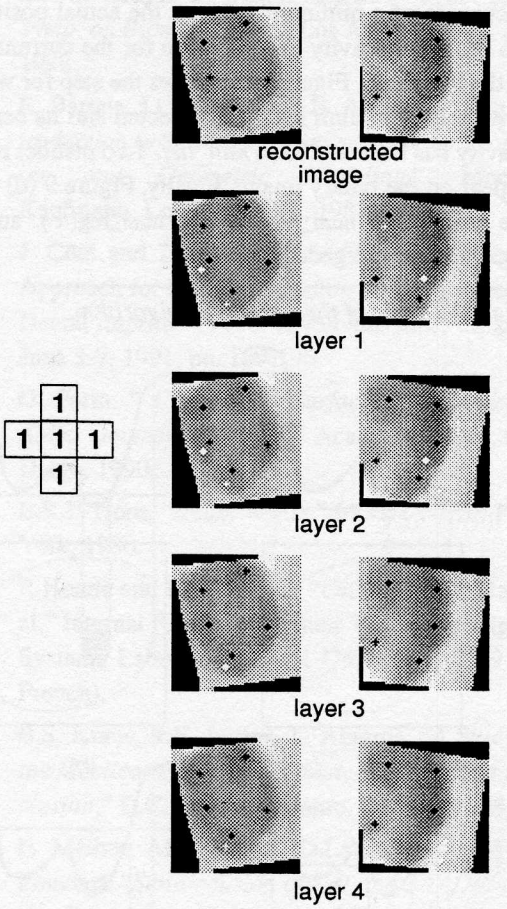

The iterative process stops when $\tau > 255$. Then, the euclidean distance $d(cg_i, cg_j)$ between each pair of points (i, j) in *min_list* is computed and the median value *med_val* of these distances is computed. Those pairs for wich $d(cg_i, cg_j) \leq (1/\varepsilon)\, med\_val$ $(0.5 < \varepsilon < 0.6)$ are detected and the point with the largest z value is kept in *min_list* while the other is discarded. This *intra-layer* processing of the distances allows for the elimination of minima caused by noise or by a poor bite on the wax imprint.

Figure 9 illustrates the basic principle of the *watershed* algorithm described above. Figure 9 (a) shows the initialization step where the global minimum of the remapped range image is detected and the coordinates are stored in *min_list*. Figure 9 (b) shows the algorithm after

several iterative steps for which num_reg $(\tau - 1)$ = num_reg(τ). The small cross that is drawn inside the region indicates the location of the first occurence of a minimum and not the actual position of the center of gravity of the region for the current value of the threshold. Figure 9 (c) shows the step for which a new local minimum has been detected and its center of gravity has been stored in *min_list*. Two distinct regions appear on the binary image. Finally, Figure 9 (d) shows the case when num_reg $(\tau - 1)$ > num_reg(τ) and two regions have merged.

Figure 9 Steps of the watershed algorithm.

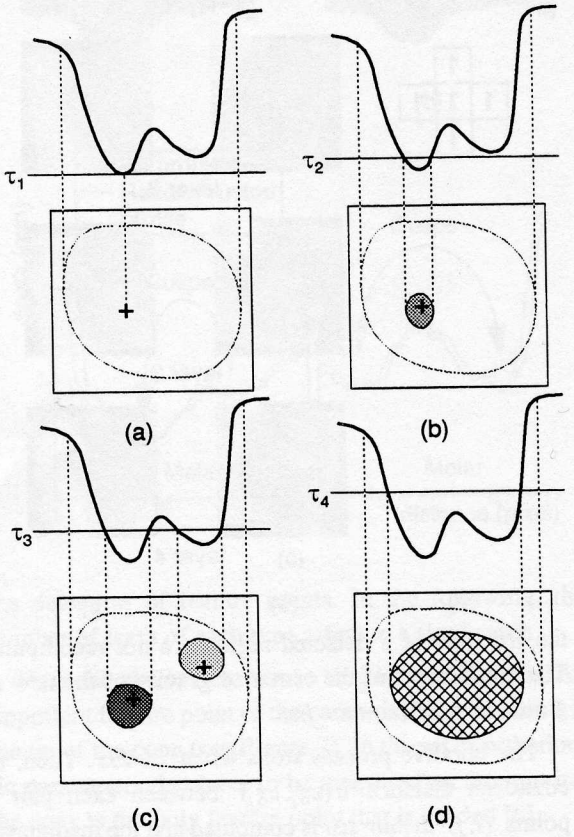

4.2.3. Scale-Space analysis for the validation of minima detection

Once the *watershed* algorithm has been applied to each of the four layers, the centers of gravity are tracked between layers. The centers of gravity detected at each layer are stored in a list called *final_list* only once (when the coordinates of a center of gravity are the same, they are not repeated in the list). The euclidean distance $d(cg_i, cg_j)$ between the each pair of points (i, j) in *final_list* is computed and the median value is computed again. Those pairs for wich $d(cg_i, cg_j) \leq (1/2)\, med\_val$ are detected and the point with the largest z value is kept in *final_list* while the other is discarded. This *inter-layer* processing of the distances allows for the elimination of minima which have moved between layers.

5. Results and discussion

Figures 8 (b) and (c) show the result for the detection of the cusps of two molars. The top image shows the final output of the *watershed* algorithm while the following images show the results at each layer. On these particular images, the white crosses show the minima that were eliminated following the *intra-layer* processing of distances between pairs of minima and the black crosses show the minima that were preserved by the algorithm[1]. The intra-layer and inter-layer processing steps thus act as some sort of voting mechanism for the detection of minima. This way, some potential errors are avoided. The validity of this method is clearly demonstrated on the top image of Figure 8 (b) and (c) since all five cusps of each molar (teeth on a mandibular arch) have been detected successfully .

Figure 10 shows experimental results for four complete arches including molars, premolars and canines (incisors need special processing that has not been implemented yet). Figure 10 (a) shows that all actual cusps and apexes have been detected for a mandibular arch. On Figure 10 (b), the cusps and apexes have been detected correctly for the teeth on a maxillary arch. The cusps and apexes have been detected correctly for the mandibular arch (Figure 10 (c)) and the maxillary arch (Figure 10 (d)) of a different dentition.

Future work will concentrate on the processing of incisors and on the extraction of the orthodontic parameters. The procedure for recording the wax imprints on subjects will be improved in order to obtain better 3-D images and thus increase the performance of the processing algorithms.

6. Acknowledgements

This research work is supported in part by a NSERC Operating Grant. Marielle Mokhtari is supported by IRIS. The authors are members of the Institute for Robotics and Intelligent Systems (IRIS) and wish to acknowledge the support of the Networks of Centres of Excellence Program of the Government of Canada, the Natural Sciences and Engineering Council, and the participation of PRECARN Associates Inc.

1. The different size of the crosses is an artefact caused by the dithering algorithm and is not the result of a poor behavior of the *watershed* algorithm.

Figure 10 Results for the cusp detection algorithm for four arches.

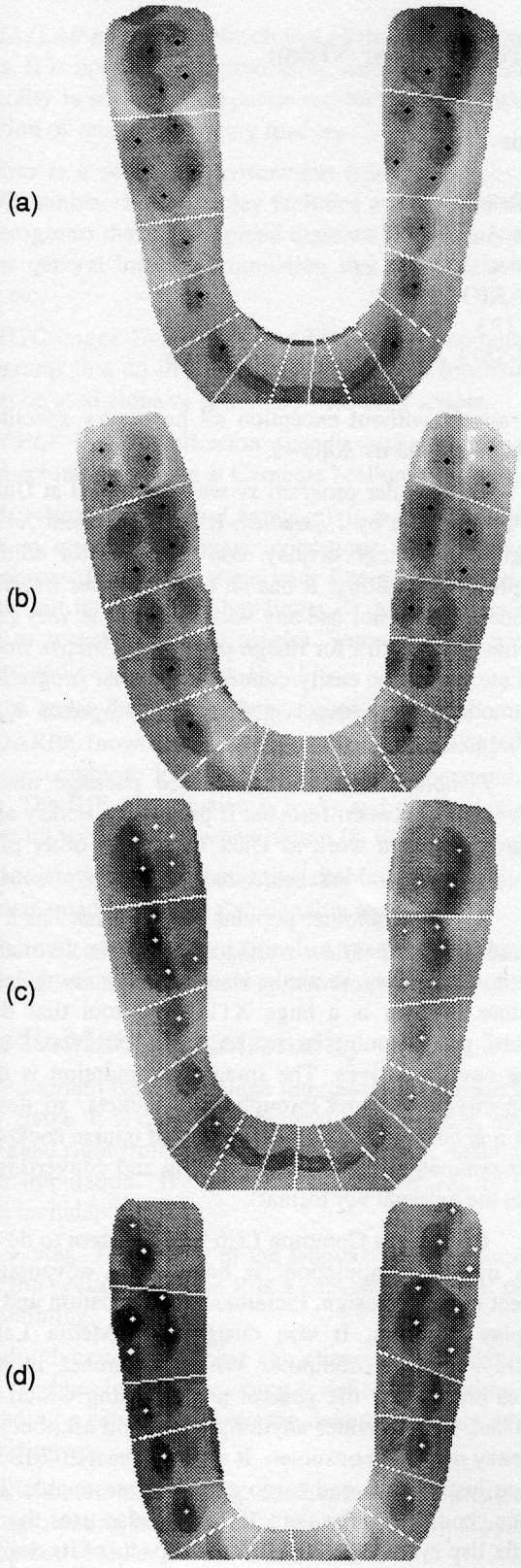

7 . References

[1] M.Aubin, D.Laurendeau, D.Poussart, "Analysis of 3-D Images of Dental Imprints," *Proc. SPIE Symp. on Biomed. Optics*, Los Angeles, Cal., Jan. 1992.

[2] R. Bartels, J.C. Beatty and B. A. Barsky, "*An Introduction to Splines for Use in Computer Graphics and Geometric Modeling*," Morgan Kaufmann, Los Altos, Cal., 1987.

[3] J. Côté and D. Laurendeau, "A Multi-Operator Approach for the Segmentation of 3-D Images of Dental Imprints", *Proc. Vision Interface*, Calgary, June 3-7, 1991, pp. 189-196.

[4] G. Farin, " *Curves and Surfaces for Computer Aided Geometric Design*," Academic Press, San Diego, 1990.

[5] B.K.P. Horn, "*Robot Vision*," McGraw-Hill, New York, 1986.

[6] R Houde and L. Guimond, "Ortho: User's Manual," Internal Report, Computer Vision and Digital Systems Laboratory, Laval University, 1989 (in French).

[7] B.S. Kraus, R.E. Jordan, L. Abrams, "*A Study of the Masticatory System Dental, Anatomy and Occlusion*," B.C. Decker, Toronto, Canada, 1988.

[8] F. Méthot, M.Mokhtari, D.Laurendeau and D. Poussart, "*Sensor fusion of 2-D and 3-D Data for the Processing of Images of Dental Imprints*," Proc. SPIE Conf. on Algorithms and Techniques, Vol 2055, Boston, Mass., Sept. 7-10, 1993.